SCIENTIFIC REPORTS

OPEN

Hydrogen physisorption based on the dissociative hydrogen chemisorption at the sulphur vacancy of MoS_2 surface

Received: 31 March 2017
Accepted: 22 June 2017
Published online: 02 August 2017

Sang Wook Han[1], Gi-Beom Cha[1], Youngsin Park[2] & S. C. Hong[1]

We provide a new insight that the sulphur-depleted MoS_2 surface can store hydrogen gas at room temperature. Our findings reveal that the sulphur-vacancy defects preferentially serve as active sites for both hydrogen chemisorption and physisorption. Unexpectedly the sulphur vacancy instantly dissociates the H_2 molecules and strongly binds the split hydrogen at the exposed Mo atoms. Thereon the additional H_2 molecule is adsorbed with enabling more hydrogen physisorption on the top sites around the sulphur vacancy. Furthermore, the increase of the sulphur vacancy on the MoS_2 surface further activates the dissociative hydrogen chemisorption than the H_2 physisorption.

For realization of the hydrogen economy, a number of strategies have been developed to tackle key technical barriers such as hydrogen generation, storage and applications in fuel cells. Especially, the most critical problem among them is to search for suitable materials that can store hydrogen at ambient temperature and atmospheric pressure[1]. During the last few decades, numerous hydrogen storage materials were extensively investigated, including carbonaceous materials[2], metal–organic frameworks[3], and metal hydrides[4]. Among them, the molecular adsorption (physisorption) on the porous materials constitutes a main avenue of research due to the fast reversibility of adsorption and desorption[5]. However, high storage densities have been obtained only at temperature of 80 K or below, because of the weak van der Waals (vdW) interaction between hydrogen molecules and the surface of most porous materials[6]. Therefore, the capacity of the H_2 physisorption at high or room temperatures is of the utmost importance.

On the other hand, the layered 2H-MoS_2 has been intensively studied as a promising and inexpensive alternative to platinum (Pt) for the prominent hydrogen evolution reaction (HER) catalysis nearing the efficiency of Pt[7], together with its unique electronic and optical properties[8]. It has long been realized that the HER activity stems from the coordinatively unsaturated sites at the edges of the MoS_2, i.e., the exposed Mo sites, while the basal plane of MoS_2 is catalytically inactive[9–11]. Hence, designing MoS_2 nanostructures with more edge sites has become a significant topic[12,13]. Very recently, the basal plane of monolayer 2H-MoS_2 has been catalytically activated and optimized for the HER by applying the strain on the single sulphur vacancies (V_S). It is understood that the dissociated hydrogen atoms or ions from the water splitting are bound at the significantly increased number of the exposed Mo atoms on the basal plane of the MoS_2[14]. More interestingly, the first-principles calculations have predicted that the H_2 molecule dissociates at the V_S[15]. Furthermore, it has been reported that the hydrogen molecules adsorb dissociatively on the 4-fold symmetric Mo exposed surface of substoichiometric MoS_x phase at room temperature[16]. These results need to reveal how the V_S on the MoS_2 surface intrinsically interacts with the hydrogen.

Since the predominant V_S defect is occasionally obtained in the MoS_2 samples prepared by mechanical exfoliation[17], we have investigated the hydrogen gas interaction on the various single-crystalline MoS_2 surfaces in the UHV chamber using angle-resolved photoemission spectroscopy (ARPES) supported by density functional theory (DFT) calculations. Here we unexpectedly find that the V_S defects serve as active sites for both hydrogen chemisorption and physisorption at room temperature. The H_2 molecules instantly and preferentially dissociate at the V_S defect on the MoS_2 surface. Additionally more H_2 molecules are adsorbed on the top site of the dissociative hydrogen chemisorption at the V_S defect with expanding the other top sites of Mo (T_{Mo}), S (T_S), and hollow, i.e., the center of a hexagon (T_H) around the V_S. This new insight makes attractive for onboard storage applications

[1]Department of Physics and EHSRC, University of Ulsan, Ulsan, 44610, Korea. [2]School of Natural Science, Ulsan National Institute of Science and Technology (UNIST), Ulsan, 44919, Korea. Correspondence and requests for materials should be addressed to S.W.H. (email: swhan72@ulsan.ac.kr) or S.C.H. (email: schong@ulsan.ac.kr)

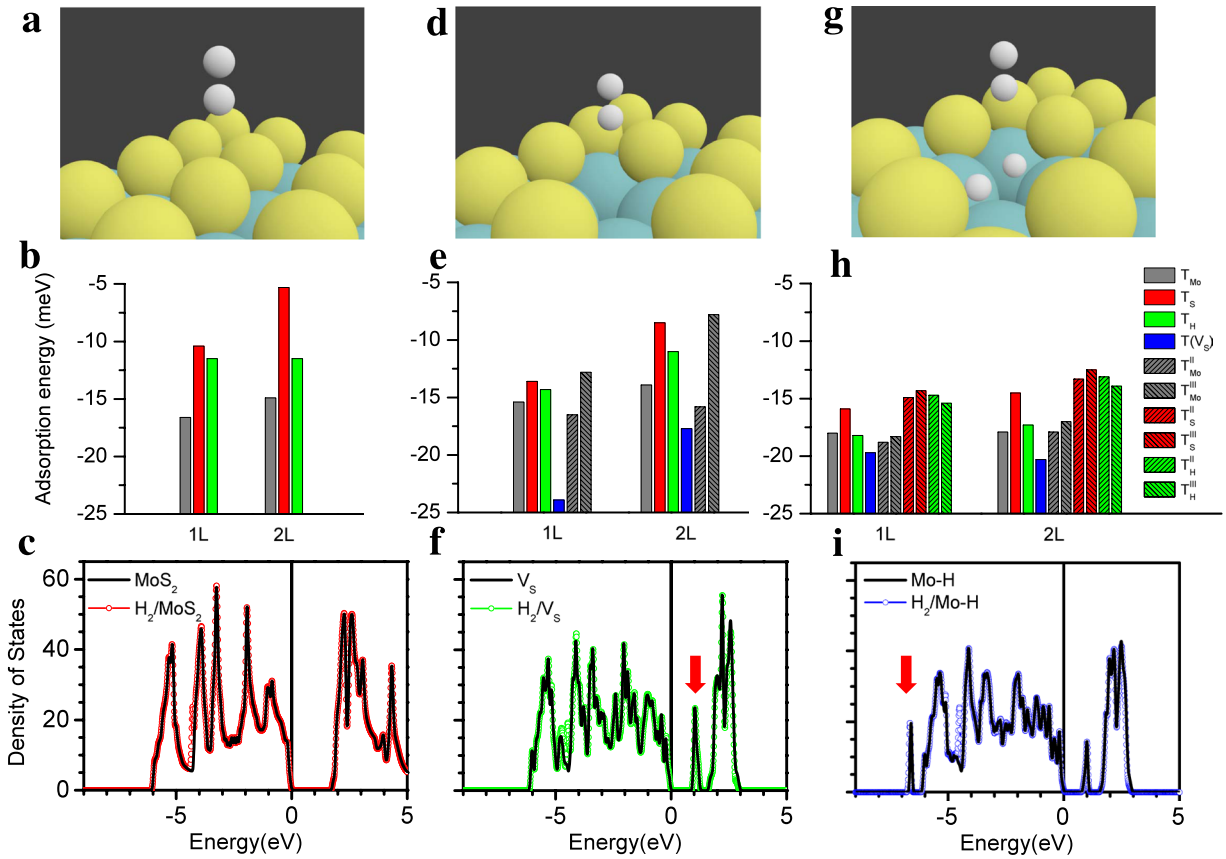

Figure 1. Enhancement of the hydrogen physisorption via the creation of a sulphur vacancy on the MoS_2 basal plane. (Upper panels) Schematic of a H_2 molecule adsorption on each surface with no defect (**a**–**c**), one S-vacancy (**d**–**f**) and two absorbed H atoms on the Mo atoms around the S-vacancy (**g**–**i**). Small (white), middle (yellow) and large (azure) balls indicate the H_2 molecule, S and Mo atoms, respectively. (Middle panels) Comparison of the adsorption energies of H_2 molecule on top of the Mo, S and hollow sites for mono- (left) and bilayer (right) MoS_2 surfaces, respectively. (Bottom panels) Comparison of the total density of states with and without the H_2 molecule adsorption. The vertical solid lines in each panel indicate the VBM being set to zero in order to clarify the bandgap.

with providing ways to modify very small specific surface area of the MoS_2 surface[18] to increase both the adsorption potential and the number of available sorption sites.

In the defect-free MoS_2 layers (Fig. 1a), the H_2 molecules favor the T_{Mo} site with having an axis perpendicular to the plane[19]. However, the other positions of T_S and T_H also have very similar adsorption energies (differences < 10 meV in Fig. 1b). The equilibrium height (h) between the center of mass of the H_2 molecule and the top Mo-layer of the MoS_2 sheet is 4.65 Å. The length of bonds in the hydrogen molecule is 0.76 Å, which is a little larger than the limiting value of 0.74 Å in the ref. 20. The adsorption of H_2 molecules on the defect-free MoS_2 surfaces has a weak contribution at −4.3 eV of total density of states (DOSs) as shown in Fig. 1c. It is notable that the interstitial H_2 molecules favor the T_H site[21].

On the other hand, when a topmost S atom is removed, i.e., the V_S defect is introduced, the preferential adsorption position of H_2 molecules changes to be the on-top site of a remained bottom S atom [$T(V_S)$] with the h[$T(Vs)$] ≈ 5.20 Å [$h(T_{Mo})$ ≈ 3.64 Å] as shown in Fig. 1d (Supplementary Fig. S1). The defect concentration is calculated using the 3×3 unit cell and estimated to be 5.56 and 2.78% for the mono- and bilayer systems, respectively. Interestingly, the on-top sites of second nearest Mo positions (T^{II}_{Mo}) surrounding the V_S have slightly lower adsorption energies than that of the first one (T_{Mo}) as shown in Fig. 1e. In addition, the difference of adsorption energies between the $T(V_S)$ and T^{II}_{Mo} sites conspicuously reduces in the bilayer than in the monolayer. More interestingly, the presence of the V_S introduces a defect state in the bandgap as indicated by (red) arrow in Fig. 1f. This new feature originates from the excess electrons of the three unsaturated Mo atoms surrounding the V_S. Nevertheless, the adsorption of H_2 molecules on the defective MoS_2 surface also has a small influence on the DOSs (Fig. 1f).

On the other hand, it has been found that the H_2 molecules dissociate at the V_S[15]. The dissociative hydrogen chemisorption is more stable with the significantly reduced adsorption energies of −0.441 eV (−0.444 eV) for monolayer (bilayer) system, compared to the physisorption of H_2 molecule at the $T(V_S)$ site (Fig. 1e). When the H_2 molecule is dissociated with distance of 1.67 Å (Fig. 1g), each H atom forms a bridge (Mo-H) bond between two Mo atoms (1.78 and 2.02 Å, respectively) of three Mo atoms around the V_S (Supplementary Fig. S2)[15]. In the

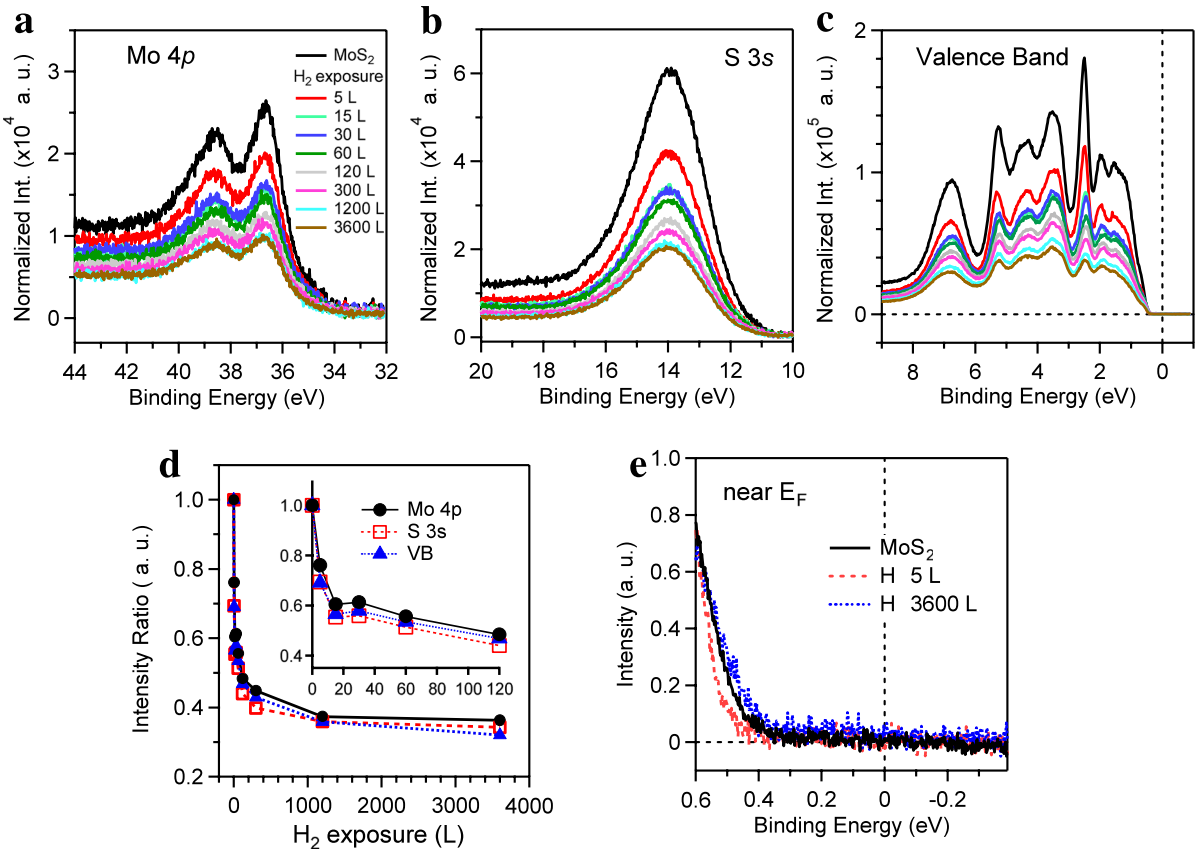

Figure 2. Reduction of the photoemission spectra by the hydrogen physisorption. Hydrogen gas adsorption on the cleaved MoS_2 surface *in-situ* at room temperature. Photoemission spectra of Mo 4p (**a**) and S 3 s (**b**) shallow core level, and valence band (**c**) were obtained at $h\nu = 100$ eV. (**d**) Plot of the relative intensity as a function of the H_2 exposure time. The inset shows a magnified region. (**c**) Valence-band maxima near the Fermi energy were obtained with high-resolution energy.

DOSs, the defect states in the bandgap (Fig. 1f) are weakened and broadened (Fig. 1i) due to the compensation of the excess electrons of the three unsaturated Mo atoms surrounding the V_S. Accordingly, the Mo-H bonds introduce additional new states at the tail of the DOSs as indicated by (red) arrow in Fig. 1i. Moreover, based on the absorbed hydrogen atoms, when the additional H_2 molecule is located on the T(V_S) site (Fig. 1h) with the $h(T_S) = 5.31$ Å [$h(T_{Mo}) = 3.80$ Å] (Supplementary Fig. S1), adsorption energies of the other positions are remarkably reduced compared to the previous case (Fig. 1g). This implies that the available adsorption sites of the H_2 molecules sequentially extend to neighboring T_{Mo}, T_H and T_S sites around the V_S defect. The H_2 physisorption based on the dissociative chemisorption (Fig. 1g) is reversely corresponds to the mechanism or reaction pathways of HER with defective MoS_2 catalysts (Volmer-Heyrowsky-Tafel mechanism).

Figure 2a–c show the shallow core-level spectra of Mo 4p and S 3 s, and the valence-band spectra, respectively. Interestingly, without the shifts of binding energies, all intensities of the photoemission spectra for the cleaved MoS_2 surface decreased rather quickly when exposed to the hydrogen gas in the UHV chamber at room temperature. In Fig. 2d, all intensities are halved in 60 s (60 L, 1 L = 10^{-6} Torr•s) and further reduced to 34% in 1 h (3600 L). The entire surface of the cleaved MoS_2 is supposed to be fully and physically covered with hydrogen gas.

In details (Fig. 2d), however, the initial H_2 exposure leads to slightly shift the valence band maximum (VBM) of the cleaved surface (0.45 eV) toward high binding energy side (0.51 eV) and then the further H_2 exposure reverses the shift of VBM toward E_F (0.43 eV). This subtle change is more elucidated in the S 2p core-level spectra (Fig. 3a). In the curve fitting, the low and high binding-energy components of the main peak represent the subsurface or bulk (161.40 eV, C_1, red solid line) and the surface (161.47 eV, C_2, blue solid line) contributions, respectively[22]. As the cleaved MoS_2 surface is exposed to the hydrogen gas, the intensity of the surface state significantly decreased from 43 to 32% (Fig. 3b), compared to the intensity change of the bulk state (from 54 to 49%). Concurrently, when the binding energy of the bulk state is fixed, that of the surface state consistently changed to follow the shift of the VBMs (Fig. 2e) with including the other components. On the other hand, we note that a very weak component is additionally required to fit the S 2p spectrum. The third component of C_3 (red triangle-dotted line) corresponds to the low-valence-state sulphur (S^-) due to the presence of the V_S defect[23]. It is away from the bulk state of C_1 by −0.75 eV, which is comparable to the energy difference between the VBM and defect state in Fig. 1f. The defect state is located at 0.78 (1.02) eV above the VBM with the bandgap of 1.25 (1.61) eV for the bilayer (monolayer). The relative intensity of the C_3 (Fig. 3b) rarely changed from 2% to 3%. This

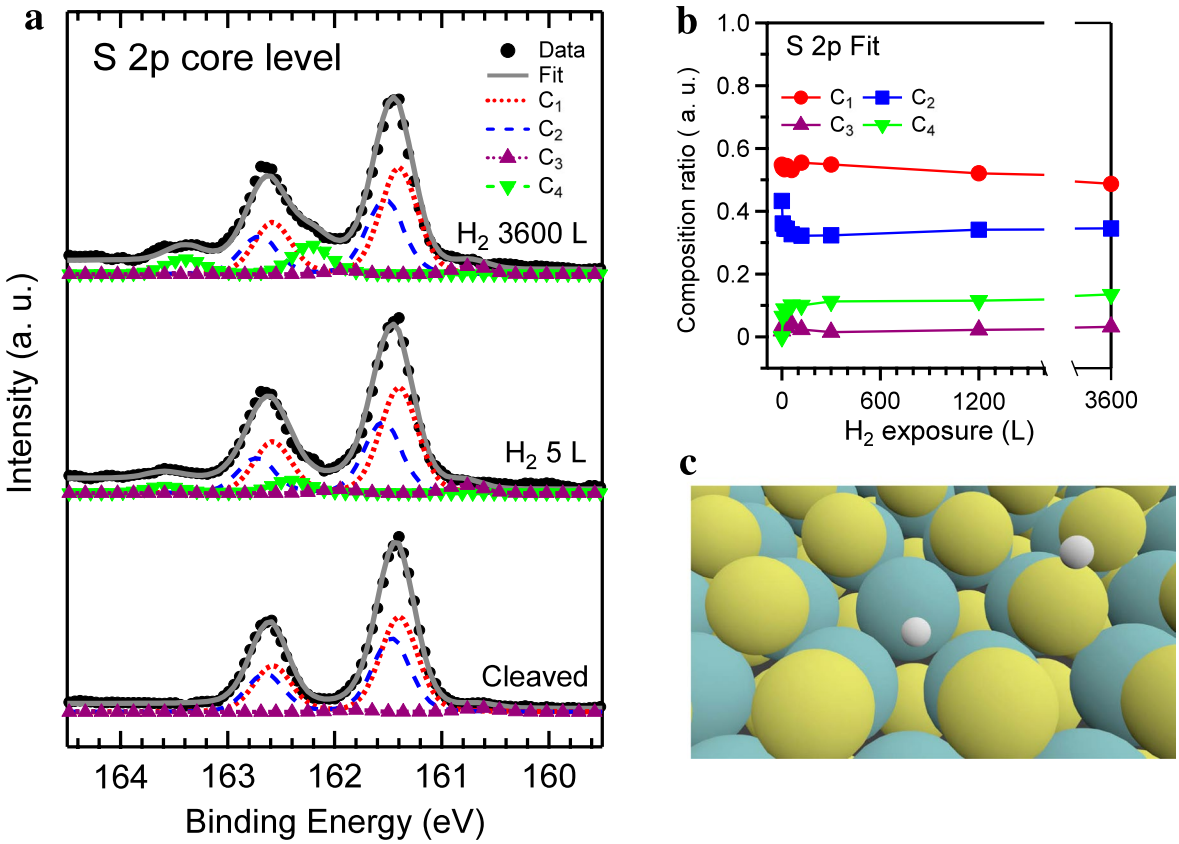

Figure 3. Evidence of the chemisorbed hydrogen at the S 2p core-level spectra. (**a**) S 2p core-level photoemission spectra (solid circles), obtained by the 2nd light order of the photon energy of 100 eV, along with the curve-fitting results. (**b**) Plot of the relative intensity for the four components, C_1 (red), C_2 (blue), C_3 (green), and C_4 (purple) as a function of the H_2 exposure time. (**c**) Schematic of two absorbed H atoms with Mo and S atoms around the S-vacancy.

amount is much larger than the estimated concentration of the V_S in the 3×3 bilayer because the probing beam size of the ARPES is approximately of 2×1 mm^2.

More importantly, a new component of C_4 (green triangle-dotted line) appeared at the higher binding energy side (162.41 eV) with the $\Delta_{SOC} = 1.18$ eV at the initial exposure of the H_2 molecules (5 L). The relative intensity further increased from 6 to 14% at the H_2 exposure of 3600 L. The energy difference between the C_1 and C_4 components (0.7~1.0 eV) is quite comparable to that (0.6 eV) between the Mo-H bonds-induced peak (−6.6 eV) and the edge of main DOSs (Fig. 1i). Thus, this new feature is considered to be related to the dissociative chemisorption of H_2 molecules (Fig. 1g) together with the VBM shift at the initial stage (Fig. 2e). On the other hand, this feature of the dissociative hydrogen chemisorption also appeared at the Mo 3d spectrum together with the S 2p spectrum when another sample was directly annealed at 300 °C in the H_2 gas ambient (Supplementary Fig. S3). This implies the formation of the mixed Mo-H and S-H (Fig. 3c) bonds around the V_S defect. The S-H bonds on the MoS_2 surface is an endothermic process with the adsorption energies of 0.656 eV, while it is an exothermic process (−0.12 eV) at the coordinatively unsaturated Mo edge sites[24]. On the other hand, it is notable that the hydrogenation of the MoS_2 single crystal by the S-H bonds induces the weak ferromagnetism and formation of the atomic stripes on the MoS_2 surface[25,26]. The further hydrogenation at higher temperature (above 500 °C) resulted in more severe decomposition of MoS_2 with H_2S desorption[27]. Thus, instead of the annealing, in order to effectively desorb the physically adsorbed H_2 molecules, the alternative method such as the application of the compressive strain is considered, because it returns to the poor activity of the basal plane[28].

On the other hand, the comparison of the ARPES data between the cleaved (Fig. 4a) and H_2 exposed (Fig. 4b) MoS_2 surfaces consistently shows delicate differences due to the hydrogen interaction. The overall band structure of the cleaved surface became diffuse after the H_2 exposure of 3600 L. The dip states (−2.35 eV) around $\overline{K}$ point in Fig. 4a, corresponding to those between the third and fourth peaks in Fig. 2c, were filled and blurred in Fig. 4b. It seems to be related to the weak contribution at −4.3 eV of DOSs due to the H_2 physisorption. Additionally, the tail of the band structures at the $\overline{\Gamma}$ point extends toward higher binding energy side. This is related to the additional new state due to the chemisorbed H atoms at the nearby Mo atoms around the V_S as shown in the DOSs of Fig. 1i and the C_4 feature in Fig. 3a.

Finally, in order to confirm the hydrogen physisorption and estimate the coverage, we performed the subsequent bismuth (Bi) deposition on the hydrogen covered MoS_2 surface. By the Bi deposition, the VBM (0.43 eV) of

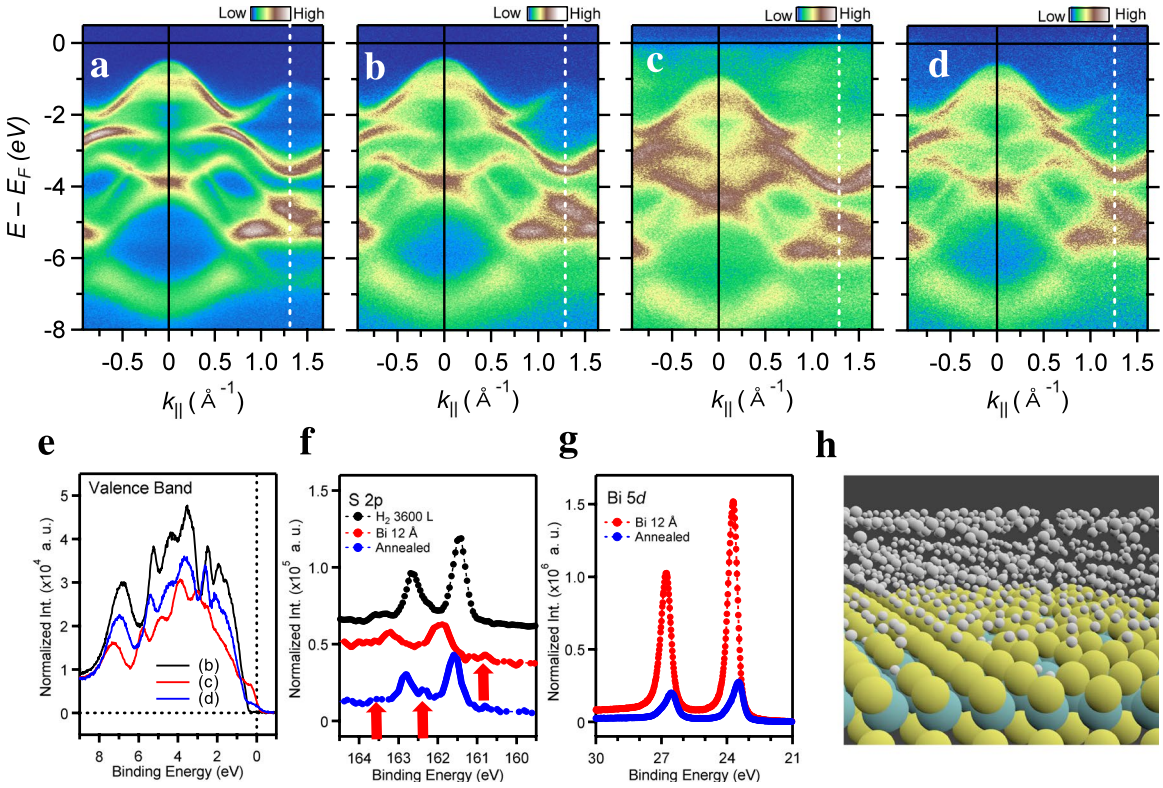

Figure 4. Estimation of the adsorbed hydrogen coverage on the MoS_2 surface. (**a**)–(**d**) ARPES intensity maps were measured along the $\overline{\Gamma K}$ high-symmetry lines before (**a**) and after (**b**) the 3600 L H_2 exposure on the cleaved MoS_2 surface, and subsequently Bi deposited on the surface of (**c**), and then annealed surface (**d**). (**e**)–(**g**) Valence band, S 2p and Bi 5d core-level spectra. (**h**) Schematic of the monolayer of physisorbed H_2 molecules based on chemisorbed H atoms on the monolayer MoS_2 with S-vacancies.

the 3600 L H_2 exposed MoS_2 surface was shifted away from E_F by 0.51 eV with partially occupied Bi related-bands at E_F (Fig. 4c), and then reversely moved toward E_F by −0.36 eV after annealing at 200 °C for 30 s (Fig. 4d). Accordingly, all the photoemission intensities were further reduced to 1/3 and then recovered to 2/3 of that before the Bi deposition (Fig. 4e and f). Notably, due to the photoionization cross section at the current photon energy[29], the partially occupied, weak contribution of the Bi p orbitals near E_F is distinct at the valence-band spectra (Fig. 4e). In addition, the C_4 feature of the S 2p spectrum was still retained even after annealing, together with the remained C_3-like feature after Bi deposition (arrows in Fig. 4f). Whereas, the intensity of the Bi 5d spectrum (Fig. 4g) was reduced to 1/5 after annealing. The ratio difference of the latter is originated from the strong hybridization of the Bi clusters on the MoS_2 surface (Details will be published elsewhere). First of all, the Bi induced electron doping into the MoS_2 surface elucidates that the H_2 molecules are adsorbed physically on the MoS_2 surface. And we notice that the reduced intensities are quite similar to the case of the Bi deposition on the cleaved MoS_2 surface, i.e., without the hydrogen exposure at the same condition of the Bi thickness (not shown here). This ensures that the desorbed H_2 molecules are no more than the monolayer, because the probing depth at the current photon energy is comparable to the thickness of 1L-MoS_2 (~6.5 Å) at least[30]. Based on these results, we could materialize the H_2 molecules covered MoS_2 surface based on the dissociative chemisorption of H atoms around the V_S defects in Fig. 4h. The heights of the physisorbed H_2 molecules are 3.57 (T_H), 7.31 (T_{Mo}), and 10.34 Å (T_S), respectively, with respect to the Mo plane. They have the tilt axes to the basal plane due to the interaction among the H_2 molecules. The estimated coverage of the H_2 physisorption on the 3×3 monolayer MoS_2, i.e., a gravimetric storage density is of 3.6 wt.%, which is much higher than the capacity of the MoS_2 nanotubes[31].

For practical application, we additionally note that the presence of the carbon impurity, especially the formation of the hydrocarbon on the air-exposed surface, is a crucial parameter to prohibit the MoS_2 surface from interacting with the hydrogen (Supplementary Fig. S4). The carbon impurity is also occasionally obtained even on the cleaved MoS_2 surfaces with having the n-type conductivity (Supplementary Fig. S3), which is contrary to the current p-type surface. In fact, the p-type feature has been more elucidated on the more defective surface[32]. Consistently, the increased V_S concentration has reduced the bandgap[14,17] and enhanced the adsorption strength on the V_S sites[14]. Moreover, the additional PES measurements and DFT calculations on the more defective MoS_2 surface (Supplementary Figs. S5 and S6) reveal that the increase of the V_S concentration further activates the dissociative hydrogen chemisorption than the H_2 physisorption. These results explain the reason of the dissociative hydrogen chemisorption at the substoichiometric MoS_x surface[16].

Our results provide a concrete possibility that the control of sulphur vacancies on the MoS_2 surface opens up a new route for the next hydrogen storage working at room temperature and possibly more capacity at lower temperature or pressure.

Methods

ARPES measurements. ARPES and photoemission experiments were performed at the 4A2 and 10D beamlines of the Pohang Accelerator Laboratory (PAL), respectively. All photoemission data were collected at room temperature. The energy and angle resolutions of the ARPES apparatus (4A2) for the ARPES data obtained at the photon energy of 100 eV were better than 130 meV and 0.4°. Natural, single crystalline MoS_2 samples (SPI) were cleaved in the UHV chamber at a base pressure better than 2×10^{-10} Torr and then exposed to the H_2 gas by filling the chamber with a pressure of 1×10^{-6} Torr. The cleanliness and structural order were verified by the quality of the valence band dispersion and low energy electron diffraction (LEED) pattern.

The S 2p core-level photoemission spectra were obtained by the 2nd light order at the photon energy of 100 eV. For comparison, they were shifted by + 101.3 eV after the energy calibration. In fitting of S 2p core-level spectra[23], the natural (Lorentzian) line width, representing the core-hole lifetime, was determined to be ~0.07 eV while the Gaussian width was fixed at the instrumental resolution of 380 meV. The values of the spin-orbit coupling (ΔE_{SOC}) and the branching ratios $I(2p_{3/2})/I(2p_{1/2})$] were 1.18 eV and 0.5, respectively.

DFT calculations. In order to understand how the presence of V_S defects fundamentally alters the catalytic property of the basal plane of MoS_2, we calculated the adsorption energies of the H_2 molecules on mono- and bilayer MoS_2 samples with and without V_S defects on each surface. The DFT calculations were performed by adopting the generalized gradient approximation (GGA) of the PBEsol[33] functional for the exchange correlation potential and the projector augmented wave (PAW) method[34] as implemented in the Vienna Ab initio Simulation Package (VASP)[35]. The electron wave function was expanded in a plane wave basis set with an energy cutoff of 400 eV. A vacuum region is thicker than 10 Å in order to avoid the coupling of the interlayer. Integration over the Brillouin zone was carried out by using $15 \times 15 \times 1$ Monkhorst-Pack k-point mesh for all systems considered. All atomic positions for 3×3 cell of mono- ($a = 3.141$ Å) and bilayer ($a = 3.142$ Å) MoS_2 were fully optimized. For comparison of the calculations with and without including the vdW interaction, the optB86b-vdW[36] functional was also calculated with the lattices of mono- ($a = 3.163$ Å) and bilayer ($a = 3.165$ Å) MoS_2 (Supplementary Fig. S7).

References

1. Schlapbach, L. & Züttel, A. Hydrogen-storage materials for mobile applications. *Nature* **414**, 353–358 (2001).
2. Xia, y., Yang, Z. & Zhu, Y. Porous carbon-based materials for hydrogen storage: advancement and challenges. *J. Mater. Chem. A* **1**, 9365–9381 (2013).
3. Zhu, Q.-L. & Xu, Q. Liquid organic and inorganic chemical hydrides for high-capacity hydrogen storage. *Energy Environ. Sci.* **8**, 478–512 (2015).
4. Yang, J., Sudik, A., Wolverton, C. & Siegel, D. J. High capacity hydrogen storage materials: attibutes for automotive applications and techniques for materials discovery. *Chem. Soc. Rev.* **39**, 656–675 (2010).
5. Bastos-Neto, M. *et al.* Assessment of hydrogen storage by physisorption in porous materials. *Energy Environ. Sci.* **5**, 8294–8303 (2012).
6. Bhatia, S. K. & Myers, A. L. Optimum conditions for adsorptive storage. *Langmuir* **22**, 1688–1700 (2006).
7. Yan, Y., Xia, B., Xu, Z. & Wang, X. Recent development of molybdenum sulfides as advanced electrocatalysts for hydrogen evolution reaction. *ACS Catalysis* **4**, 1693–1705 (2014).
8. Wang, W. H., Kalantar-Zadeh, K., Kis, A., Coleman, J. N. & Strano, M. S. Electronics and optoelectronics of two-dimensional transition metal dichalcogenides. *Nature Nanotech.* **7**, 699–712 (2012).
9. Salmeron, M., Somorjai, G. A., Wold, A., Chianelli, R. & Liang, K. S. The adsorption and binding of thiophene, butane and H_2S on the basal plane of MoS_2 single crystals. *Chem. Phys. Lett.* **90**, 105–107 (1982).
10. Hinnemann, B. *et al.* Biomimetic hydrogen evolution: MoS_2 nanoparticles as catalyst for hydrogen evolution. *J. Am. Chem. Soc.* **127**, 5308–5309 (2005).
11. Jaramillo, T. F. *et al.* Identification of active edge sites for electrochemical H_2 evolution from MoS_2 nanocatalysts. *Science* **317**, 100–102 (2007).
12. Kibsgaard, J., Chen, Z., Reinecke, B. N. & Jaramillo, T. F. Engineering the surface structure of MoS_2 to preferentially expose active edge sites for electrocatalysis. *Nature Mater.* **11**, 963–969 (2012).
13. Xie, J. F. *et al.* Defect-rich MoS_2 ultrathin nanosheets with additional active edge sites for enhanced electrocatalytic hydrogen evolution. *Adv. Mater.* **25**, 5807–5813 (2013).
14. Li, H. *et al.* Activating and optimizing MoS_2 basal planes for hydrogen evolution through the formation of strained Sulphur vacancies. *Nature Mater.* **15**, 48–53 (2016).
15. Li, H., Huang, M. & Cao, G. Markedly different adsorption behaviors of gas molecules on defective monolayer MoS_2: a first-principles study. *Phys. Chem. Chem. Phys.* **18**, 15110–15117 (2016).
16. Bao, Y. *et al.* Substoichiometric molybdenum sulfide phases with catalytically active basal planes. *J. Am. Chem. Soc.* **138**, 14121–14128 (2016).
17. Hong, J. *et al.* Exploring atomic defects in molybdenum disulphide monolayers. *Nature Commun.* **6**, 6293 (2015).
18. Polyakov, M. *et al.* W. Hydrocarbon reactions on MoS_2 revistied, I: Activation of MoS_2 and interaction with hydrogen studied by transient kinetic experiments. *Journal of Catalysis* **256**, 126–136 (2008).
19. Ye, Q., Shao, Z., Chan, S. & Li, J. Adsorption of gas molecules on monolayer MoS_2 and effect of applied electric field. *Nano Res. Lett.* **8**, 425 (2013).
20. Lide, D.R. *CRC Handbook of Chemistry and Physics*, CRC Press, 88th ed. (2007).
21. Zhu, Z., Peelaers, H. & Van de Walle, C. G. Hydrogen intercalation in MoS_2. *Phys. Rev. B* **94**, 085426 (2016).
22. Han, S. W. *et al.* Band-gap transition induced by interlayer van der Waals interaction in MoS_2. *Phys Rev. B* **84**, 045409 (2011).
23. Duchet, J. C., van Oers, E. M., de Beer, V. H. J. & Prins, R. Carbon-supported sulfide catalysts. *Journal of Catalysis* **80**, 386–402 (1983).
24. Prodhomme, P.-Y., Raybaud, P. & Toulhoat, H. Free-energy profiles along reduction pathways of MoS_2 M-edge and S-edge by dihydrogen: A first-principles study. *Journal of Catalysis* **280**, 178–195 (2011).
25. Han, S. W. *et al.* Controlling ferromagnetic easy axis in a layered MoS_2 single crystal. *Phys. Rev. Lett.* **110**, 247201 (2013).
26. Han, S. W. *et al.* Hydrogenation-induced atomic stripes on the 2H-MoS_2 surface. *Phys. Rev. B* **92**, 241303(R) (2015).
27. Ye, G. *et al.* Defects engineered monolayer MoS_2 for improved hydrogen evolution reaction. *Nano Lett.* **16**, 1097–1103 (2016).

28. Chen, X. & Wang, G. Tuning the hydrogen evolution activity of MoS_2 (M = Mo or Nb) monolayers by strain engineering. *Phys. Chem. Chem. Phys.* **18**, 9388–9395 (2016).
29. Yeh, J. J. & Lindau, I. Atomic subshell photoionization cross sections and asymmetry paramters: 1<=Z<=103. At. *Data Nucl. Data Tables* **32**, 1–155 (1985).
30. Han, S. W. *et al*. Band-gap expansion in the surface-localized electronic structure of MoS_2 (0002). *Phys. Rev. B* **86**, 115105 (2012).
31. Chen, J., Kuriyama, N., Yuan, H., Takeshita, H. T. & Saki, T. Electrochemical hydrogen storage in MoS_2 nanotubes. *J. Am. Chem. Soc.* **123**, 11813–11814 (2001).
32. Addou, R. *et al*. Impurities and electronic property variations of natural MoS_2 crystal surfaces. *ACS Nano* **9**, 9124–9133 (2015).
33. Perdew, J. P. *et al*. Restoring the density-gradient expansion for exchange in solids and surfaces. *Phys. Rev. Lett.* **100**, 136406 (2008).
34. Blöchl, P. E. Projector augmented-wave method. *Phys. Rev. B* **50**, 17953 (1994).
35. Kresse, G. & Furthmüller, J. Efficient interative shemes for ab initio total-energy calculations using a plane-wave basis set. *Phys. Rev. B* **54**, 11169 (1996).
36. Klimeš, J., Bowler, D. R. & Mechaelides, A. Van der Waals density functionals applied to solids. *Phys. Rev. B* **83**, 195131 (2011).

Acknowledgements

S.W.H. especially thanks to Prof. Dr. Sunmin Ryu (POSTECH) for his valuable discussion. This work was supported by the Priority Research Centers Program and Basic Science Research Program through the National Research Foundation of Korea (NRF) funded by the Ministry of Education (Grant Nos. 2009-0093818, 2015R1A2A2A01003621, 2015R1D1A1A01058332, 2017R1D1A1B03030740). Experiments at PLS were supported by MSIP and PAL of Korea.

Author Contributions

S.W.H. designed and analyzed the data. Y.S.P. & S.W.H. performed the photoemission and ARPES measurements. S.W.H. wrote the manuscript. G.B.C. & S.C.H performed the DFT calculations. All authors contributed to analyze and interpret the data and to writing the manuscript.

Additional Information

Supplementary information accompanies this paper at doi:10.1038/s41598-017-07178-9

Competing Interests: The authors declare that they have no competing interests.

Publisher's note: Springer Nature remains neutral with regard to jurisdictional claims in published maps and institutional affiliations.